JOURNAL OF GEOPHYSICAL RESEARCH, VOL. 105, NO. C12, PAGES 28,695–28,708, DECEMBER 15, 2000

Study of the dynamics of wind-driven transports into the Yellow Sea during winter

S. K. Riedlinger and G. A. Jacobs

Naval Research Laboratory, Stennis Space Center, Mississippi

Abstract. Synoptic wind stresses and surface heat flux force a three-dimensional numerical ocean model of the Yellow Sea/East China Sea dynamics. The basin response to winter winds is examined through the model output fields. Northerly wind bursts are a frequent winter occurrence in this region. The wind bursts develop a southward flowing current along the Chinese coast as the wind stress forces fluid out of the Bohai Sea. A north-south pressure gradient develops as surface water travels from the Bohai Sea southward, decreasing the elevation in the north relative to the elevation in the south. Also, a westward pressure gradient across the Yellow Sea basin develops in response to the wind forcing. The southward pressure gradient forces a bottom flow in the direction opposite to the wind stress. This return flow is concentrated in a deep trough located on the eastern side of the basin. After the northerly wind ceases the northward transport increases pressure in the north with the result of slowing or stopping the flow northward. At times, pressure increases in the north sufficiently to force a southward flow in the trough. Following strong northerly wind events, northward transport into the Yellow Sea occupies the entire trough and may extend into the northern Yellow Sea/Bohai Sea. During periods of calm winds, northward flow usually does not penetrate beyond 34°N in the Yellow Sea. This flow is northward on the western side of the island of Cheju. The flow turns eastward north of Cheju and then southward, passing through the Cheju-Korea Strait. The wind stress along the Korean coast often deviates from the northerly wind stress over the rest of the Yellow Sea. Thus the flow along the Korean coast is not as closely related to the northerly wind bursts as the flow along the Chinese coast. The winter circulation in the Yellow Sea is predominately a barotropic response to winds with fluctuations due to Ekman flow.

1. Introduction

The Yellow Sea is a shallow semienclosed sea, bounded in the east by the Korean peninsula and in the west by the Chinese coast. To the north is the very shallow Bohai Sea, and to the south lies the deeper East China Sea, with the deep Pacific water farther south. In the central Yellow Sea lies a trough of about 90 m depth, which aligns with the north-south axis of the basin. A shallow, gently sloping shelf lies along the Chinese coast, while the Korean coastal shelf drops rather sharply into the trough.

This region is very dynamic with a strong boundary current, the Kuroshio, in the southern section; strong tidal interactions; large rivers discharging considerable fresh water in the summer; and strong atmospheric forcing. Each of these factors contributes to the diverse character of the region. Several water masses have been identified from historic hydrographic data [*Su and Weng*, 1994; *Liu et al*., 1992; *Hur et al*., 1999]. They include the warm, saline Kuroshio waters; the cold, fresher coastal water; the cold Yellow Sea Bottom Water; the Yangtze Dilute Water; and various modified water types. Satellite data and images are useful in determining location of fronts, eddies, and to some degree, general circulation. Thermal fronts around the Shandong Peninsula, along the southern Chinese coast (Zhejiang and Fujian provinces), and along the southern coast of Korea and the warm tongue in the central Yellow Sea are readily discerned from satellite images. The persistence of these fronts suggests the existence of mean currents [*Zheng and Klemas*, 1982].

Satellite data and in situ data show the characteristics of the Yellow Sea for restricted area and for short periods of time. Numerical models can examine the entire region for very long time periods to give a more complete view of the basin and dynamical interactions. In addition, components of the fundamental momentum equations may be analyzed individually. Thus the importance of each dynamical component may be evaluated throughout the region. Several two-dimensional (2-D) barotropic numerical models have been developed to study the region.

Prior 2-D models [*Le et al*., 1993; *Wang and Yuan*, 1988; *Hsueh et al*., 1986; *Choi*, 1982] agree on several aspects of the wind-driven barotropic circulation. *Choi* [1982] and *Hsueh et al*. [1986], using different numerical methods, showed that a northward flow in the Yellow Sea trough during winter is related to northerly wind events. The numerical model of *Hsueh et al*. [1986] further showed a southward pressure gradient develop in response to a northerly wind. Model elevation drops in the north (Bohai Sea) in response to a northerly wind event. In addition, an increase in sea level along the Chinese coast and southward coastal currents along the Chinese coast and nearshore along the Korean coast develop as well. Following the peak of the winds, the relaxation of the pressure gradient results in an upwind flow in the deeper water of the Yellow Sea trough. Hsueh et al.'s model results suggest that

Paper number 2000JC900127.

short time period fluctuations (<7 days) appeared to be related to frontal passage and the winds associated with them, while longer period fluctuations were related to fluctuations in the Kuroshio. *Wang and Yuan* [1988] performed several simulations with an idealized basin. They showed that a northward (upwind) flow in the trough could be formed from northerly wind stress alone, without the Kuroshio and heat fluxes. The flow field can attain near–steady state conditions when the northerly wind lasts for about 1 day. When the wind relaxes or disappears, the circulation is variable. Southward flow along the Chinese and Korean coasts is also associated with the northerly wind and northward flow in the trough. *Wang and Yuan* [1988] further suggested that the warm tongue often observed in the trough was more likely due to more rapid cooling in the shallow coastal areas than to advection of warm water northward. Their short-term simulations (~72 hours) did not show northward heat advection with the upwind current. *Le et al*. [1993] used a 2-D vertically averaged numeral model with realistic basin geometry and winter wind fields to examine the winter circulation in the Yellow Sea and Bohai Sea region. The basic features of winter circulation from their simulations were a northward flow in the trough following the northerly winds, southward coastal currents along China and Korea, a cyclonic gyre on the west side of the Yellow Sea, and an anticyclonic gyre on the east side of the southern Yellow Sea. They surmised that circulation in the Yellow Sea was predominately wind-driven and that open boundary conditions (e.g., the Kuroshio) had little influence north of 32°N.

The northward flow in the Yellow Sea trough has generally been referred to as the Yellow Sea Warm Current (YSWC). *Uda* [1934] was the first to recognize this current and to suggest that it was a branch of an eastward flowing current along the continental shelf in the East China Sea. There has been much debate and conflicting definitions as some authors define the YSWC by water mass properties (temperature and salinity) and others define it by a northward flow (velocity) in the trough. *Lie* [1984], *Hsueh* [1988], and *Liu et al*. [1992] show that using the water mass definition, the YSWC does not extend farther northward than 34°N in winter, thus calling into question whether the northward flow in the trough in winter should be called the YSWC. *Hsueh and Yuan* [1997] refined the *Hsueh et al*. [1986] model by including surface heat fluxes. Even though they were not able to reproduce temperature distributions satisfactorily, they showed that particle trajectories calculated from the model velocity resulted in northward displacement of particles, implying a northward transfer of heat. *Mask et al*. [1998], using the same 3-D numerical model used in this paper, examined the water mass definition and northward flow definition of the YSWC and the effect of wind stress on each of these views of the YSWC. They concluded that there is a northward flowing current with or without winds but that this flow is about an order of magnitude weaker without winds than with winds. Model results also show that using the water mass definition of the YSWC ($S > 33.5‰$ and $12 < T < 21$°C [*Su and Weng*, 1994]), it penetrates as far as 34°N with winds in winter (similar to previously discussed models) but no farther. Without winds it does not exceed 33°N. They also concluded that the simulation was greatly influenced by open boundary conditions (i.e., the Taiwan Warm Current, the Kuroshio, and the river inflows in summer) and the winds act to steer the current and add a pulse-like flow to the current. They suggested calling the northward flow, which travels along the trough in the Yellow Sea, the Yellow Sea Warm Current and calling the water mass usually associated with it the Yellow Sea Warm Intrusion.

The barotropic models discussed above have provided some insight into the interaction of the winds and currents in winter. These 2-D models reproduce the vertically integrated basic basin response. However, in reality the Yellow Sea region is 3-D, and there is some vertical variation in the basin even in winter. In this study we use a 3-D numerical model with realistic bottom topography, coastal configuration, temperature and salinity distribution, and atmospheric forcing to examine vertical as well as horizontal variations in the basin currents in winter. Results are similar to the prior 2-D models, indicating that the response is mainly barotropic, though the subsurface northward current in response to the northerly wind stress indicates a strengthening before the northerly winds begin to dissipate.

The model boundary conditions, atmospheric forcing, and related specifics of the model are discussed in section 2. Evaluation of the model relative to earlier barotropic models of the region and comparison to satellite and in situ data is discussed in section 3. Barotropic response to selected winds events is discussed in section 3. The 3-D response of the model to wind forcing and comparison of this response to in situ measurements are discussed in section 4. The model experiment covers 3 years. We examine model climatology (3 year averages) to evaluate the model general circulation. Also, we focus on the second year of the model simulation, when start-up transients have died down. The transport variations across the entrance to the Yellow Sea are compared to the area-averaged wind stress and pressure differences between the Yellow Sea and the East China Seas in section 4. In addition, the statistical relation between these variables is examined through a time-lagged cross-covariance analysis. We then closely examine the variations during one northerly wind event. Last, the forcing mechanisms that appear to dominate the process of upwind flow following northerly wind bursts are discussed in section 5. Conclusions are given in section 6.

2. Model Description

In this study we use a numerical dynamic/thermodynamic model of the Yellow and East China Seas based on the Princeton Ocean Model [*Blumberg and Mellor*, 1987]. The model region (Figure 1) includes the Bohai Sea, Yellow Sea, and East China Sea with an extension into the deep Pacific to allow inflow and outflow of the Kuroshio Current system. The model uses a rectilinear, horizontal grid with variable spacing from 25 to 8 km, and the model grid is rotated 39° from true north (Figure 1). There are 24 sigma levels vertically to a maximum allowed depth of 2000 m. Bottom topography for the model region is shown in Figure 2. The southeastern model boundary (south of the Ryukyu Islands) is closed to transport. The Taiwan Strait, Korean Strait, and the Kuroshio south of Taiwan and Japan are open boundaries. Transport for the Kuroshio is set to 23 Sv south of Taiwan and 22 Sv south of Japan [*Zhao and Fang*, 1991]. The vertical distribution of temperature and salinity at the boundaries for the Kuroshio are based on historical studies [*Nitani*, 1972]. Winter and summer temperature and salinity are set at the inflow ports. In the Korean Strait, transport varies from 2 Sv in winter to 4 Sv in summer. Transport through the Taiwan Strait is set to be 1 Sv less than that in the Korean Strait [*Fang et al*., 1991]. At the Taiwan Strait the temperature and salinity boundary conditions vary seasonally.

Monthly temperature and salinity values are applied at the Korean boundary.

Temperature and salinity boundary values are applied via upstream advection boundary technique using boundary values if inflow and modeled values if outflow. Velocity distribution at the inflow/outflow boundary of the Kuroshio is determined from geostrophic calculations using the inflow temperature and salinity profiles. At the open boundaries the Kuroshio is assumed to extend over four grid points (~100 km width). A parabolic velocity distribution is also assumed across the Kuroshio and to a level of no motion of 600 m. The velocities are then scaled so that the inflow velocity yields a transport of 23 Sv and the outflow velocity yields a transport of 22 Sv. The velocity at the Taiwan Strait is assumed to be barotropic with a uniform distribution of velocity across the strait and with depth. Korean strait outflow is distributed across 16 grid points in the form of two jets each 4 grid points wide. The jet on the Japan side of the strait is the stronger of the two. All boundary values are interpolated to model time steps.

Atmospheric forcing is from the Navy Operational Global Atmospheric Prediction System (NOGAPS) [*Hogan and Rosmond*, 1991]. The NOGAPS data horizontal resolution is 1.25° × 1.25°. The data fields are provided at a frequency of once per day, and the model experiment interpolates between the daily values. Wind stress, surface air temperature, and vapor pressure are used to determine the surface momentum flux and the surface heat flux for forcing the model. The air temperature and vapor pressure, along with monthly cloud cover values, are used to compute from bulk formula the surface heat fluxes [*Parkinson and Washington*, 1979; *Gill*, 1982; *Walker and Mey*, 1988]. A solar radiation formula dependent on global position, time of year, time of day, and a midlatitude albedo is used to compute the surface incoming solar radiation [*List*, 1958; *Reed*, 1977]. Solar extinction with depth within the water column is obtained from a 3 bandwidth formulation [*Morel and Antoine*, 1994]. The model is initialized with January climatological temperature and salinity developed at the Naval Oceanographic Office (NAVOCEANO). Surface elevations and velocities are initially zero. Freshwater inflow from five regional rivers is part of the external forcing. Monthly mean values for the Yangtze, Yellow, Liahoe, Yalu, and Han were taken from the World Meteorological Organization's (WMO) version of the United Nations Educational, Scientific, and Cultural Organization's (UNESCO) data set. A maximum monthly flow rate of 54,100 $m^3 s^{-1}$ for the Yangtze occurs in July. The minimum for this river occurs in January (9280 $m^3 s^{-1}$). The Yellow River, the next largest river, has a maximum runoff of 4380 $m^3 s^{-1}$ in September and a minimum runoff of 640 $m^3 s^{-1}$ in December. The other rivers are much smaller. All forcing and boundary inputs are linearly interpolated to the model time step. The model simulation is run with climatological boundary forcing and NOGAPS atmospheric forcing from the years 1993–1995. The model with the forcing develops a Kuroshio Current in the East China Sea, coastal currents, and reasonable temperature and salinity distributions. In winter, temperatures are near or at freezing in portions of the Bohai Sea and increase southward to reach values in the 20°C range. The Bohai and Yellow Seas are vertically homogeneous. Coastal water is several degrees colder than central Yellow Sea water. This warmer water forms a tongue-like feature in the trough region. In the summer, surface temperatures warm to exceed 20°C over the entire region. At depth, in the Yellow Sea a much colder bottom water forms. The salinity from the river outflow forms low-salinity coastal waters. The Yangtze outflow remains close to the coast of China during winter but extends out into the East China Sea during summer, forming a tongue-like feature that reaches to near Cheju.

For this study, no tidal elevations or tidal currents are applied at the boundaries. Tidal-induced vertical mixing and currents can affect temperature and salinity distribution in the region, particularly during summer [*Beardsley et al.*, 1983; *Lie*, 1989; *Seung et al.*, 1990; *Shin and Seung*, 1993; *Lee and Choi*,

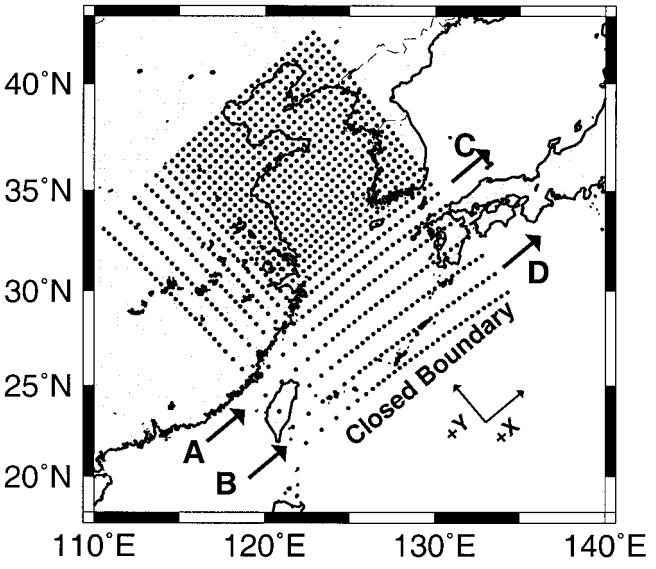

Figure 1. Yellow Sea/East China Sea model grid. Every fifth point is shown. A, B, C, and D denote open boundaries. The southern boundary is closed.

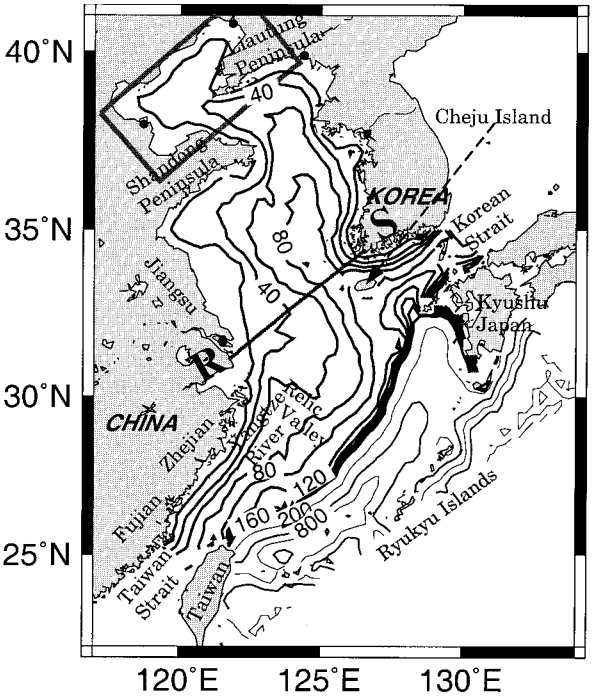

Figure 2. Model bathymetry (m) and position of transect RS. Box denotes area where Bohai Sea elevation average is calculated. Dots denote positions of river input.

1997]. However, since we are only examining the response to wind stress over short time periods, the small variations in density will not have a large impact on the results. Understanding the individual effects before combining the forcing sources is important.

3. Model Evaluation

Previous studies with this model indicate the model's capability to generate the short time period and sea surface height variations associated with wind stress. Comparison of satellite-observed surface height, in situ pressure gauge measurements, and model surface height [*Jacobs et al*., 1998b] indicates that the model reproduces short time period sea level events in the region. Model events are in phase with observed events. For the largest events the model peak anomalies are not as large as those observed. This may be due to the NOGAPS wind stress not containing sufficiently strong winds. Continental shelf waves are generated by winds and propagate southward from the Bohai Sea along the Chinese coast [*Jacobs et al*., 1998a]. These coastal waves are observed in both the satellite data and the model results, and the results agree favorably in terms of amplitude and wavelength. Both the model and observations imply a propagation speed of 12 m s^{-1}. Further analysis of in situ pressure gauge data and model elevation results in the northern Yellow Sea indicates that spectral coherence is significant down to periods of 3 days and that the phase difference is near 0. Near the shelf break the coherence is significant down to 5 day periods. There is very little energy at time periods shorter than these.

NOGAPS winds, model surface elevation, and ocean currents at depths of 5 and 50 m averaged over February for the 3 years of model simulation are shown in Figure 3. The winds are predominately northerly (Figure 3a), typical for winter. The model reproduces many of the general circulation patterns described by previous investigators. The model contains a well-developed Kuroshio in the southern East China Sea located along the 200 m isobaths. The Kuroshio is evident in the sea surface elevation plot (Figure 3b). Inflow from the Yellow Sea on the north side of the Bohai Strait and outflow on the south side of the strait is present in the model 5 m currents (Figure 3c) [*Miao and Liu*, 1989]. *Miao and Liu* [1989] show that this flow is a result of northerly winds. This flow is reversed under the influence of southerly winds. Southward flow around the Shandong Peninsula and along the Chinese coast (Figure 3c) is similar to that observed by *Zheng and Klemas* [1982], *Beardsley et al*. [1985], and *Chen et al*. [1994]. This current is weak nearshore and strengthens offshore. A portion of this flow turns eastward into the East China Sea near the mouth of the Yangtze River, forming a cyclonic gyre. The remaining flow continues southward as a narrow current along the Chinese coast. A year-round cyclonic gyre (eddy) similar to the modeled gyre was discovered by *Hu et al*. [1980] and furthered studied by *Mao et al*. [1983]. The gyre was centered at 31°30′N, 125°30′E. *Mao et al*. [1983] showed that the gyre intensified and moved south in winter when the Chinese Coastal Current and the Yellow Sea Warm Current were strong. It weakened and moved northward in summer when the currents were weaker. More recently, *Qingge et al*. [1998] showed a cyclonic eddy southwest of Cheju by using sequential advanced very high resolution radiometer satellite images. Along the Korean coast the model generates a southward current that continues around the southern Korean coast and into the Korea Strait. A branch of this current turns westward near the southwestern tip of Korea and extends into the Yellow Sea. At 5 m, northward flow in the Yellow Sea trough appears to be an extension of the flow from the gyre in the East China Sea and the Korean Coastal Current. At 50 m, northward flow is strong in the Yellow Sea trough. This flow extends into the northern Yellow Sea. The Tsushima Warm Current (TsWC) appears in the mean currents as flowing northward from the Kuroshio west of Kyushu and passing through the Korean Strait. This is evident at 5 and 50 m in the model mean currents. The Taiwan Warm Current (TWC) flows from the Taiwan Strait eastward across the East China Sea shelf. A small portion of the flow turns northward into the Yangtze relict river valley and then along the shelf before turning north and flowing into the Yellow Sea west of Cheju (Figure 3d). The mean model circulation is similar to that deduced from historic data. In particular, the mean currents resemble the schematics of *Beardsley et al*. [1985] and *Chen et al*. [1994]. We do not try to ascertain the origin of currents like the YSWC or the TsWC in this paper. We concentrate on the wind forcing of currents in the Yellow Sea. Studies to better understand the distribution of TWC water and Kuroshio water in the Yellow Sea are discussed by *Hur et al*. [1999] and *Jacobs et al*. [2000].

Much of the mean circulation can be reproduced with barotropic numerical models [*Hsueh et al*., 1986; *Hsueh*, 1988; *Wang and Yuan*, 1988; *Le et al*., 1993]. One important result from barotropic models is the development of a southward pressure gradient in response to a northerly wind. The relaxation of the pressure gradient, following the peak of the wind, results in a northward flow into the Yellow Sea. The pressure gradient develops as sea level begins to drop in the north (Bohai) in response to a northerly wind event. This sea level drop occurs in conjunction with an increase in sea level along the Chinese coast and southward coastal currents along the Chinese and Korean coasts. The strength of these currents depends on the strength of the wind stress.

The response of our 3-D model to two northerly wind events in early April 1994 is examined (Figure 4) and compared to prior barotropic results. April is rather late in the year for comparison to previous models since the previous 2-D models considered winter conditions. This time period was chosen, however, since the northerly wind events were preceded by several days of weak southerly winds. The sea level was relatively flat and currents were weak. Thus little to no effect of earlier northerly wind events is evident. Also, the region was not yet strongly stratified. The model reference frame is rotated 39° from true north (Figure 1) to allow local coastal features to be oriented more parallel to the numerical grid. For convenience we refer to the X and Y components of wind stress and northward and eastward currents in the local model reference frame. The Y component of the NOGAPS wind stress is averaged for the area north of transect RS (Figure 2). This area-averaged wind stress value ($\bar{\tau}_y$) is used to infer the strength of the southerly wind stress. Northerly wind bursts appear as negative values of $\bar{\tau}_y$. The time series of $\bar{\tau}_y$ for 11 days in April 1994 (Figure 4a) contains two northerly wind events. The mean elevation in the Bohai Sea for this time period ($\bar{\eta}_B$, Figure 4b) gives a measure of the strength of the southward pressure gradient since the height variations in the East China Sea are relatively small. Elevation in the Bohai Sea decreases as the northerly wind stress increases and reaches a peak anomaly ~12 hours following the peak northerly winds stress. The elevation decrease is greater in the second event,

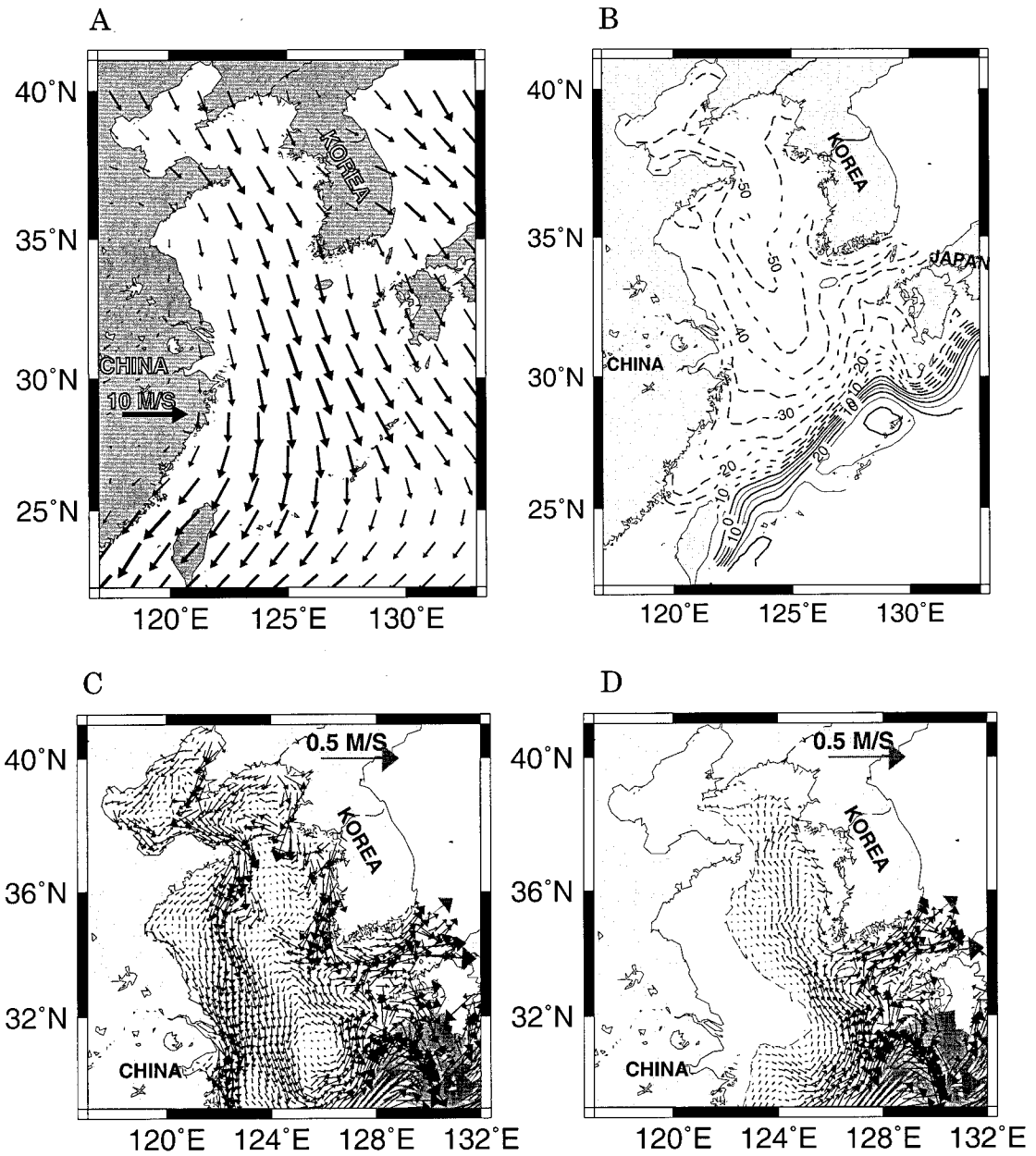

Figure 3. February average over 3 years, 1993–1995: (a) NOGAPS winds, (b) model-simulated surface elevation, (c) model current velocity at 5 m, and (d) model current velocity at 50 m. Vectors of magnitude >0.3 m s^{-1} are shaded.

which has stronger wind stress. Elevation rebounds between the northerly wind events during the period when the winds are weak. Northward transport (Figure 4c) in the Yellow Sea trough along transect RS remains small until after the peak of the northerly wind because the wind stress balances the pressure gradient until after the wind stress peaks. At this time, there no longer is a force balancing the pressure gradient, and the fluid accelerates northward. The northward transport increases the elevation in the north, eventually shutting down the northward flow. The northward transport may overcompensate and cause southward transport.

4. Three-Dimensional Response to a Northerly Wind Event

The 3-D numerical model results are very similar to those obtained by 2-D models, both in mean circulation and in barotropic response to northerly wind events. Now we examine the vertical variations in the response to wind events by examining the sea surface height and currents at 5 and 50 m in response to one particular wind stress event. Then the statistical relations between velocity, wind stress, and sea surface height provide insight into the general response. Finally, some in situ measurements are compared to model results.

4.1. Description of an Event

The wind stress, model currents at 5 and 50 m, and surface elevation from day 95 (April 5) through day 99 (April 9) of 1994 are compared (Plate 1). This time period covers the first wind event examined in Figure 4. The wind stress on day 95 (Plate 1a) is weak and predominately southeasterly. The next day, a strong northerly wind progresses southward from the Bohai Sea, covering the whole region by day 97 except for the

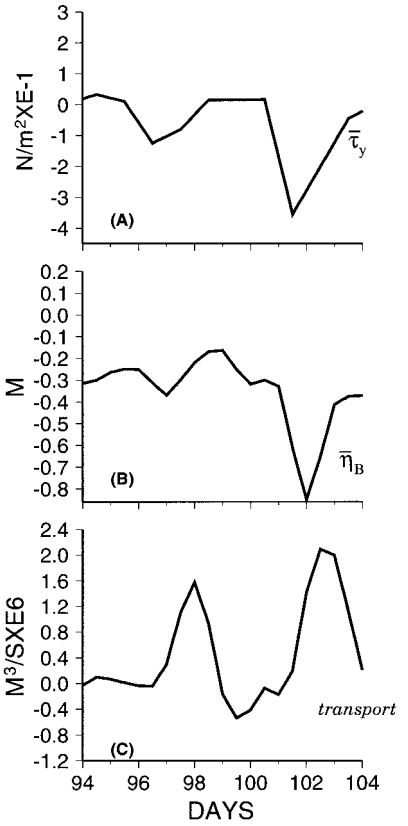

Figure 4. (a) North-south wind stress averaged over the Bohai Sea and Yellow Sea, $\bar{\tau}_y$, (b) averaged elevation in Bohai Sea, $\bar{\eta}_B$, and (c) transport in the trough, surface to bottom (124°–126°E along transect RS) for a period in April that contains two northerly wind events.

easterly winds over the Korean peninsula. The winds change direction to easterly over the Yellow Sea by day 98 and continue easterly through day 99.

On day 95 the model currents at 5 m (Plate 1b) indicate northward flow along the Chinese and Korean coasts. The flow along the Korean coast turns counterclockwise to the Shandong Peninsula and joins the flow out of Bohai Sea. Flow within Bohai Sea is clockwise. Water flows southward around the tip of the Shandong Peninsula and then flows southward in the Yellow Sea between the 40 and 60 m depth contours. At 31°N the southward flow joins the eastward flow across the East China Sea, with some of the flow turning north entering the central Yellow Sea. Flow in the East China Sea is eastward across the shelf. On day 96 in the Bohai Sea and northern Yellow Sea, the 5 m currents have southwestward flow with increased outflow around the Shandong Peninsula. Southward currents strengthen and move close to the Chinese coast. Along the Korean coast, flow changes to southward nearshore and northward offshore. There is an east to west flow in the central Yellow Sea. On day 97 flow develops into a general counterclockwise configuration in the Yellow and East China Seas: northward along the Korean coast, eastward in the northern Yellow Sea, and then southward around the Shandong Peninsula continuing along the Chinese coast. This pattern persists into day 99 but weakens considerably.

The currents at 50 m on day 95 (Plate 1c) contain weak southward flow in the Yellow Sea. At the entrance to the Yellow Sea near Cheju, flow is northward on the west side of the island. The northward flow penetrates to about 34°N before it turns southward and flows through the strait between Cheju and Korea. On day 96, there is little change in the flow in the southern Yellow Sea, but in the north, flow out of Bohai Sea occurs. By day 97 the flow out of the Bohai Sea continues south along the 50 m contour on the west side and is met by northward flow that encompasses much of the eastern part of the basin. This flow pattern continues into day 98 but is weakened. On day 99, flow is out of the Yellow Sea, as flow north and west of Cheju is predominately southward.

The surface elevation (Plate 1d) on day 95 is low in the north relative to the south. The variation is no more the 20 cm within the Yellow Sea and Bohai Sea from north to south and <10 cm from east to west. A minimum of -40 cm occurs southwest of Cheju. On day 96, there is an increase in elevation on the south side of the Bohai Sea and a decrease on the north side. The wind stress (Plate 1a) initially forces mass from the north to the south. Elevations in the East China Sea do not significantly change, but elevation begins to increase along the Chinese coast and decrease in the central Yellow Sea. On day 97 the elevation gradients become quite strong in the Yellow Sea. An elevation low approximately parallel to the basin's north-south axis in the central Yellow Sea deepens to -50 cm. During day 97 the southward gradient is strongest and corresponds to the strong northward flow at 50 m (Plate 1c) on this day. The gradient along the Chinese coast is much greater than that along the Korean coast. As the northerly wind relaxes during days 98 and 99, the Bohai Sea elevation increases, and the gradient across the sea dissipates. The gradient along the Chinese coast also decreases.

The 3-D response shows a time lag between the surface and deeper flow. The 50 m currents peak during day 97, when the wind stress and southward pressure gradients are largest. The peak northward flow at 5 m occurs during day 98, after the wind stress has relaxed. Thus the northward deep transport begins during the peak wind stress, while the near-surface transport is still southward and under the influence of the winds.

4.2. Relation Between Winds, SSH, and Currents

We construct a statistical comparison to more rigorously evaluate the relations between the forcing and the response. Cross correlations are examined among the 1994 time series' spatially averaged wind stress ($\bar{\tau}_y$ as described in section 3), model results of the mean elevation in the Bohai Sea ($\bar{\eta}_B$), transport along the Chinese coast, transport in the Yellow Sea trough, and transport along the Korean coast. (Note that model output is sampled at 3 hour intervals for this analysis.) The transports are taken along a model grid line RS (Figure 2). This model grid line roughly defines the separation between the Yellow Sea and the East China Sea. This transect transverses the gentle sloping coastal shelf on the Chinese side, the trough in the central Yellow Sea, and the steeper coastal shelf along the Korean coast (Figure 5). Along transect RS the maximum depth is 91 m and the average depth is 44 m.

The transport along the Chinese coast is defined here as the transport integrated from surface to bottom and integrated from the Chinese coast to 123°E along transect RS. This covers the region of major southward flow observed in section 4.1. The transport in the Yellow Sea trough is integrated from the bottom to 40 m along transect RS where bottom depth is more than 40 m. The transport along Korea is integrated over all depths and integrated from the Korean coast to 126°E along transect RS.

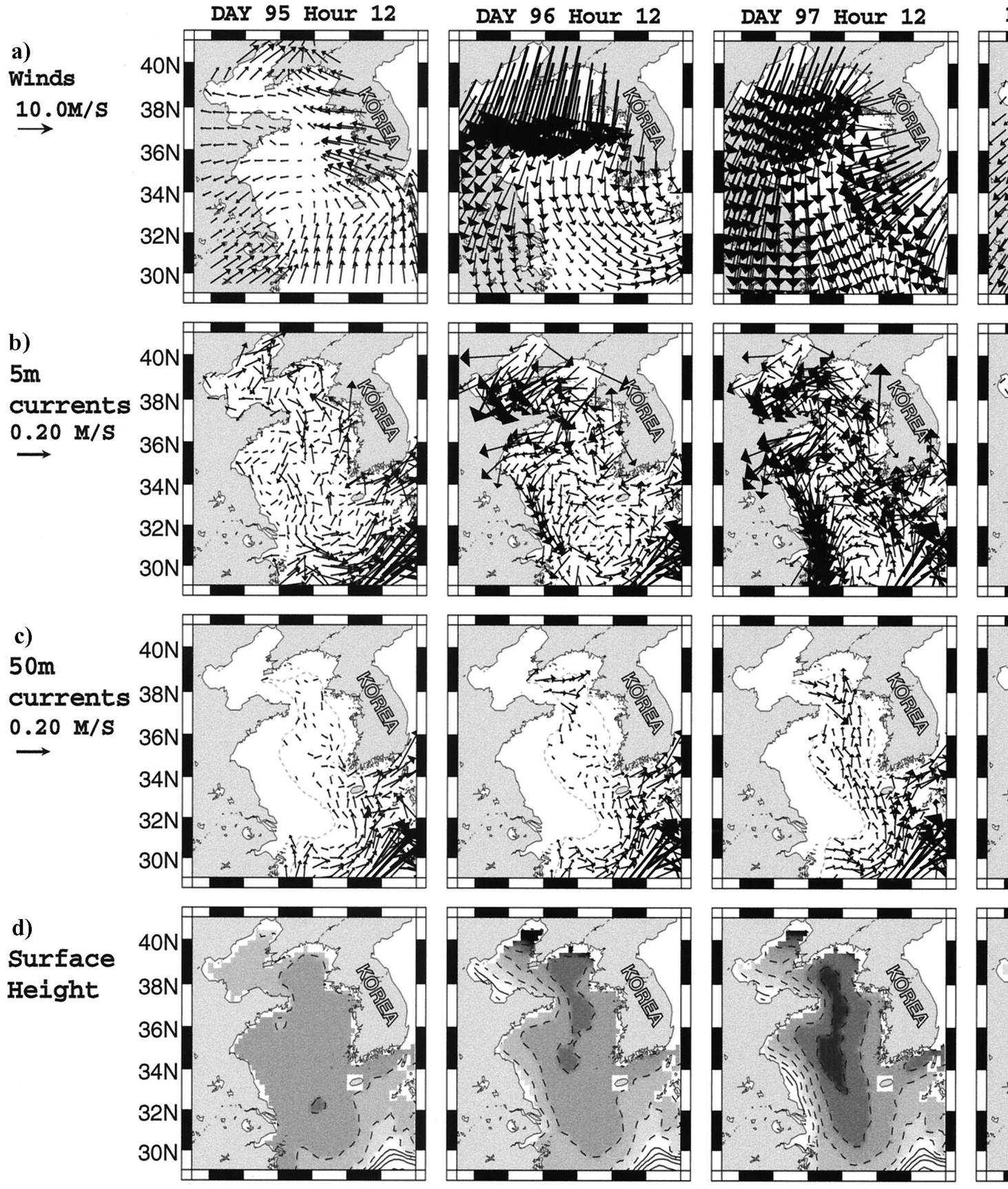

Plate 1: a) **Surface winds, b) mo**
at 50 m depth, and d) su
day 95 to 99. Negative s

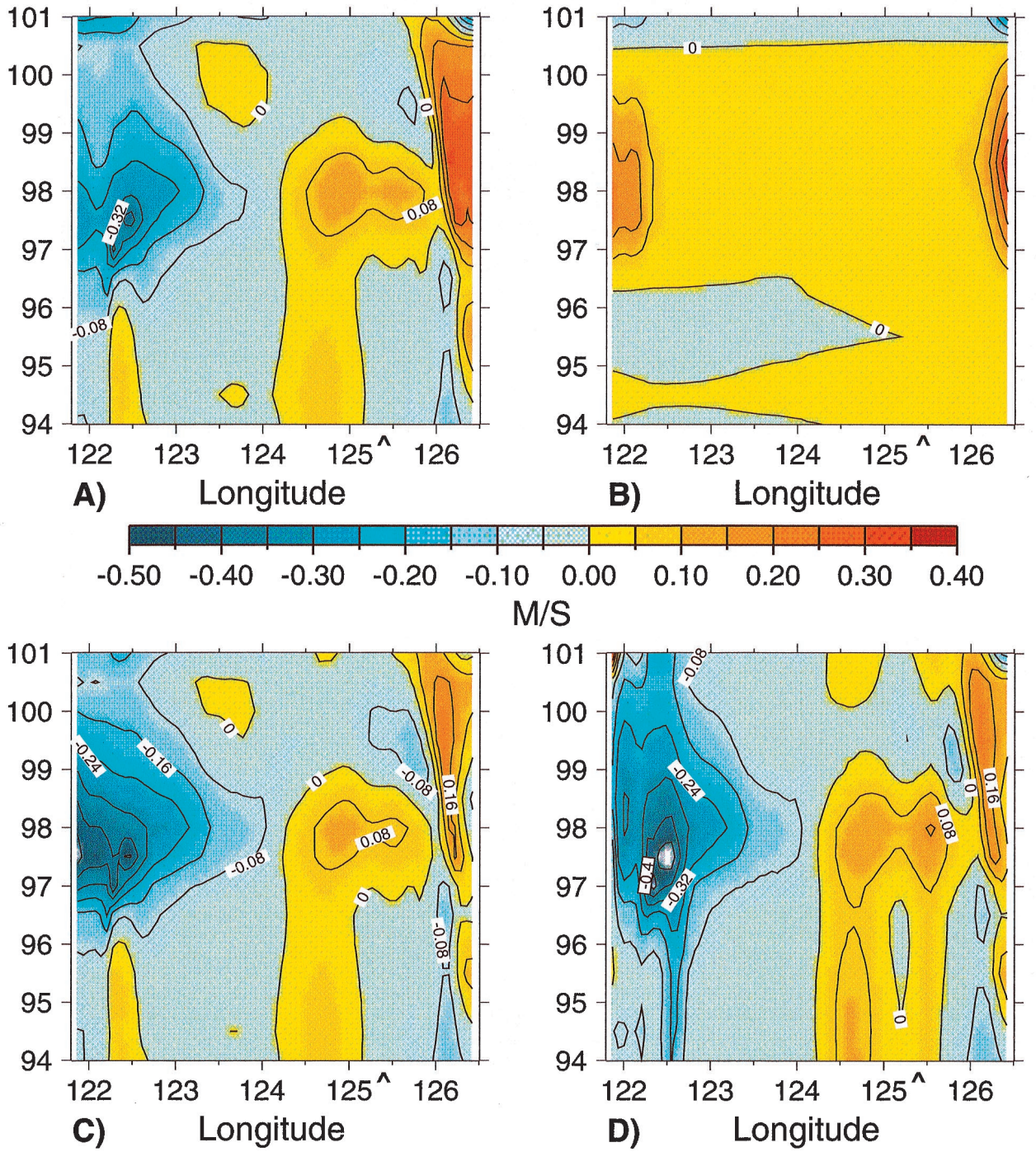

Plate 2. Model response along transect RS from day 94 to day 101: (a) vertically integrated northward velocity, (b) northward Ekman velocity, (c) vertically integrated northward velocity minus the Ekman velocity, and (d) geostrophic velocity computed from model elevations along RS (m s^{-1}). The carets denote the deepest point along transect RS.

The stress $\bar{\tau}_y$ has a correlation of 0.73 with $\bar{\eta}_B$ and leads the elevation changes by about 12 hours (Figure 6a). Also, $\bar{\tau}_y$ has a 0.68 correlation with the transport along the Chinese coast and precedes the transport by about 9 hours (Figure 6b). The correlation between $\bar{\tau}_y$ and the transport in the trough is −0.56 with the wind stress leading the transport by about 24 hours (Figure 6c). In addition, cross correlation between $\bar{\tau}_y$ and transport along the Korean coast is 0.31 with the wind stress leading transport by 6–9 hours (Figure 6d). The X component of the wind stress is better correlated than $\bar{\tau}_y$ with the transport along the Korean coast (−0.51 and a lag of 21 hours).

These lagged correlations lead to a view of the typical response to the wind stress. A northerly wind event (negative $\bar{\tau}_y$) initially generates a southward surface transport. The southward transport begins to drain the Bohai Sea, thus depressing the elevation. The peak sea surface height drop in the Bohai Sea occurs 12 hours after the peak wind stress. This elevation drop in the Bohai Sea creates a pressure gradient that accel-

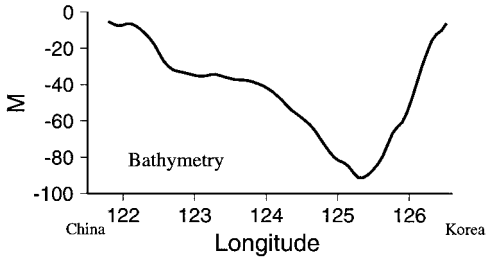

Figure 5. Bathymetry along transect RS shown in Figure 2.

erates flow northward. About 24 hours following the peak northerly wind stress the peak northward transport occurs in the Yellow Sea trough. The transports along the coasts do not indicate a significant northward flow in response to the pressure gradient because wind stress counteracts the pressure gradient. However, the Yellow Sea trough is deep enough to be isolated from the wind stress. The contribution of the flow along the Korean coast does not appear to play as large of a role in this process as the flow along the Chinese coast. The Korean coastal current appears as an Ekman-driven current that lags the easterly wind stress by 21 hours.

4.3. In Situ Measurements

The Naval Oceanographic Office, in the summer of 1995, deployed several acoustic Doppler current profilers (ADCPs) and pressure gauges in the Yellow Sea and East China Sea. The instruments were bottom moored in special trawl resistant mounts [*Teague et al*., 1998] since the intense level of fishing in the region usually results in low retrieval rates of instruments. These instruments recorded measurements through the winter of 1995–1996. In Figure 7 the positions of two of the moorings in the Yellow Sea trough (diamonds) and one model point along transect RS (square) are shown. Line plots for site A and site C depict sea level (from the pressure field), near-surface currents (14 m at sites A and C), midlevel currents (38 m at site A and 44 m at site C), and near-bottom currents (70 m at site A and 72 m at site C). (The currents are thin solid, thin dotted, and thin dashed lines.) The mean currents are computed after the removal of tidal currents from the ADCP record. Also shown is the *Y* component of NOGAPS wind at the two mooring sites (thick solid line) and the sea level represented by pressure changes (thick dashed line). At site C, the northernmost site, two northerly wind events occur. The sea level variation at this point indicates a decrease in sea level as the strength of the northerly wind increases. The currents change from southward to northward. Flows at each level react together, indicating a uniform flow with depth. The lag time between the peak wind and the peak northward flow is about 12 hours for the first event and about 36 hours for the second event. There appears to be a shorter lag time with stronger winds. At site A, west of Cheju, one northerly wind event is shown. The near-surface flow does not switch from southward to northward after the peak of the wind but decreases to near zero. The subsurface currents change to northward following the peak northerly wind, with the peak northward velocity at 70 m lagging the peak current at 38 m. The lag time between the peak of the wind and the peak northward flow at depth is about 48 hours. Model currents for the chosen point along RS

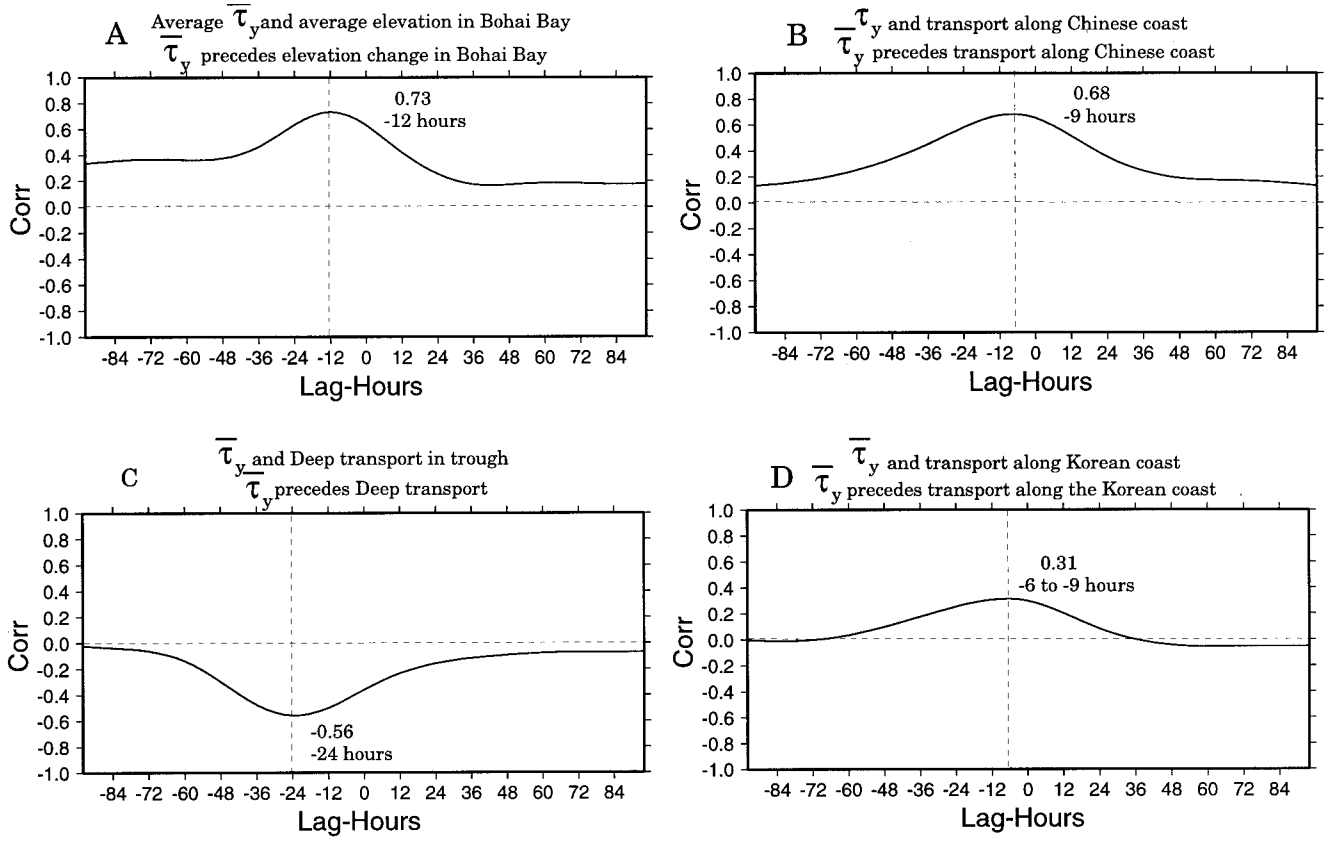

Figure 6. Cross correlation of area-averaged $\bar{\tau}_y$ with (a) area-averaged elevation in Bohai Sea $\bar{\eta}_B$, (b) transport along the Chinese coast, (c) transport in the trough, and (d) transport along the Korean coast.

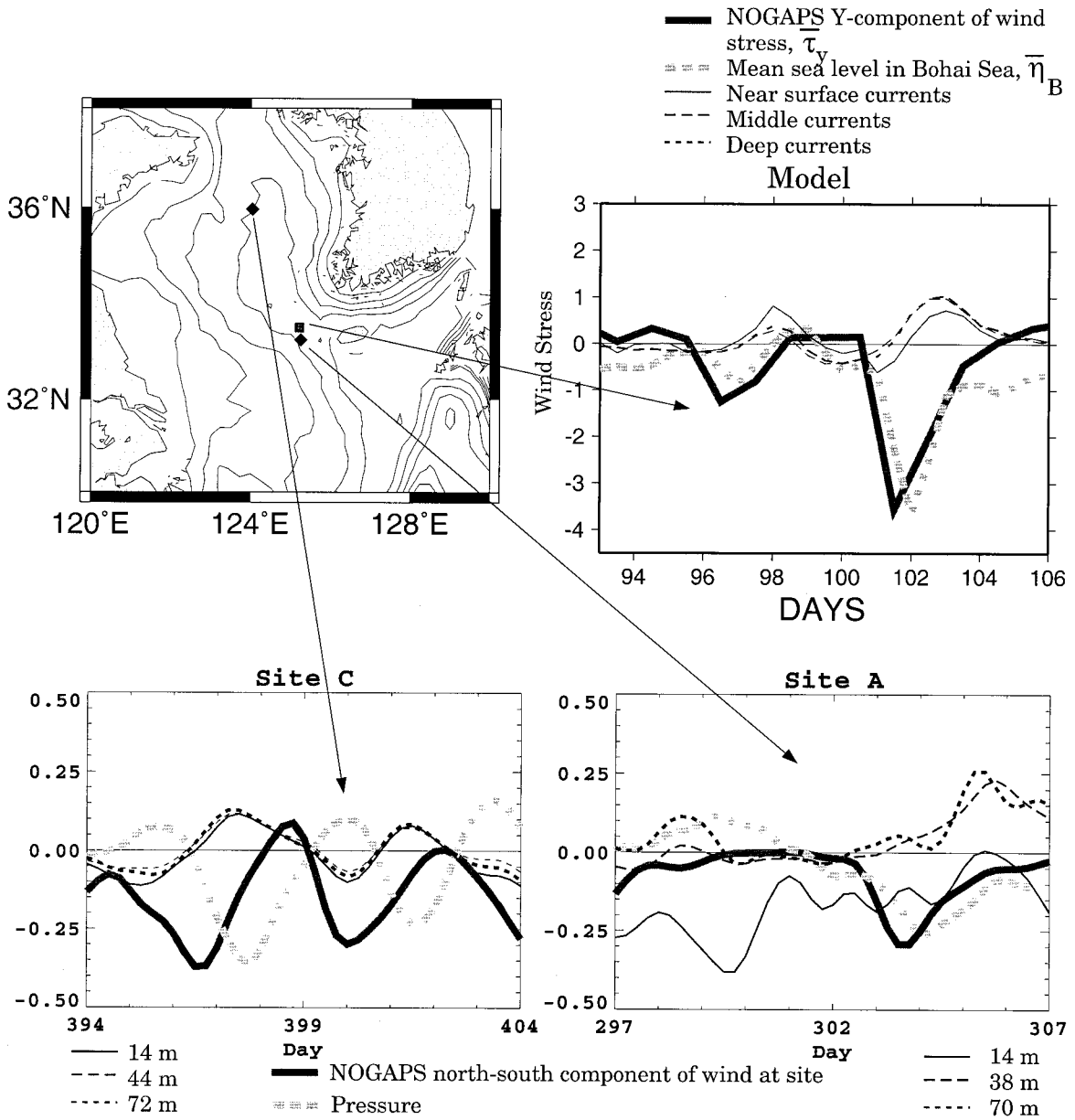

Figure 7. Position of three sites in the Yellow Sea used to compare model and in situ data. Model results are computed at the site denoted by the square. The diamonds denote sites A and C where ADCPs and pressure gauges were deployed. The thick solid line in each plot shows the NOGAPS wind stress. The thick dashed line shows the sea level from model or pressure measurements. The thin lines depict currents: near-surface (solid line), middle (dashed line), and deep (dotted line) currents. Plots for sites A and C are courtesy of W. J. Teague, Naval Research Laboratory, Stennis Space Center, Mississippi.

are vertically averaged for the surface (0–10 m depth), middle (10–40 m depth), and deep (40 m to bottom). The NOGAPS Y component $\bar{\tau}_y$ and the elevation $\bar{\eta}_B$ from Figure 4 are also shown in the plot. Model results show the northward currents following the peak northerly wind are the same as the in situ data. The model elevation $\bar{\eta}_B$ peak value has a shorter lag time between it and the peak northerly wind $\bar{\tau}_y$ than do the in situ results of winds stress and pressure. The model site shows results simulated for early April 1994: site A shows 10 days in September–October 1995, and site C shows 10 days in January–February 1996. Even though each site shows results from different wintertime periods, the interaction between winds, elevation, and currents are the same. This implies that the wind and pressure effects are basin-wide and are a frequent winter occurrence.

5. Dynamics

The significance of various forcing sources to the dynamical balance across transect RS is examined from the point of view of the linearized vertically integrated (barotropic) equations of motion

$$\frac{\partial u}{\partial t} = fv - \frac{\partial p}{\partial x} + F_{Bx} + F_{Sx}$$

$$\frac{\partial v}{\partial t} = -fu - \frac{\partial p}{\partial y} + F_{By} + F_{Sy},$$

where the Coriolis parameter is f, the vertically averaged velocity is (u, v), the bottom friction is represented by the vector

$(\mathbf{F}_{Bx}, \mathbf{F}_{By})$, and the surface forcing is represented by the vector $(\mathbf{F}_{Sx}, \mathbf{F}_{Sy})$. The effect of surface forcing may be measured by the Ekman velocity, which is the depth-averaged velocity induced by the Ekman transport

$$V_{EK} = -\frac{\tau_x}{\rho f H},$$

where ρ is water density and H is water depth. If the Ekman velocity is subtracted from the vertically averaged velocity, the remainder is referred to as the pressure velocity and is forced by bottom friction, pressure, and the Coriolis force. If bottom friction is small, in steady state the pressure velocity is in geostrophic balance.

To examine the individual forcing contributions to the transport, we compare the vertically averaged velocity across transect RS (Plate 2a) to the Ekman velocity (Plate 2b), the pressure velocity (Plate 2c), and the geostrophic velocity across transect RS (Plate 2d). The averaged velocity contains the peak southward transport along the Chinese coast during day 97, the northward transport across the trough during days 97–98, and the large northward transport along the Korean coast during days 97–100. By separating the different contributions to the averaged velocity we attempt to understand which mechanisms are dominant in different areas.

The Ekman velocity is mostly northward and strongest along the Korean coast over days 97–99. Ekman transport contributes to northward flow in the trough and opposes the southward transport along the Chinese coast. Along the Korean coast the Ekman velocity is a significant contributor to the averaged velocity. With the Ekman velocity removed, flow at the Korean coast is southward on day 98, as indicated by the pressure velocity (Plate 2c). On the Korean side the contribution of Ekman velocity is larger than the flow from other forces. Along the Chinese coast, between days 97 and 99, the southward pressure velocity increases to a maximum of 0.48 m s^{-1}, and the Ekman flow considerably reduces this southward flow. In the central Yellow Sea the Ekman velocity does not have a large effect on the total velocity, but a noticeable decrease in velocity occurs in the trough around day 98 when the Ekman velocity is removed.

Geostrophic velocity is computed from the elevation along transect RS

$$V_g = \frac{g}{f}\frac{\partial \eta}{\partial x},$$

where η is elevation. The geostrophic velocity (Plate 2d) is similar in many respects to the pressure velocity (Plate 2c). The geostrophic velocity indicates the northward maximum off the Korean coast from days 97 through 100. This northward transport appears in the pressure velocity as well. The implication is that the dynamical balance of this particular feature is mainly a geostrophic balance and that the northward Ekman transport in this instance intensifies the event. The northward flow at 124.5°E from days 94 through 96 and the northward flow across the trough during days 97 and 98 appear to be in near-geostrophic balance.

The southward flow along the Chinese coast during days 96–99 is partially in geostrophic balance, though the peak geostrophic velocity amplitude is larger and slightly farther from shore than the pressure velocity. Close to the coast, surface Ekman velocity and bottom friction alter the geostrophic flow. Before day 96, between longitude 122° and 123°E, geostrophic velocity indicates a southward flow, and the pressure velocity indicates a northward flow. Wind stress and pressure gradients are much weaker during this time period. Thus forces other than geostrophy and northward Ekman drift cause the northward flow here. The contributors to this flow would be the nonlinear terms disregarded in the simplified analysis. Thus advection of momentum could be one additional effect. Also, bottom stress as well as thermohaline effects from the Yangtze River, which is near by, could have a significant effect here. On the east side of the trough, at 125.5° a northward geostrophic flow also appears that is countered by dynamics not considered here.

To understand the geostrophic implied velocity over the domain during the development of this event, we compute the geostrophic currents from the sea level elevation in Plate 1d. On day 95 the geostrophic current computed from the sea level elevations (Figure 8) contains features very similar to the current at 5 m (Plate 1b). These include the clockwise circulation in the Bohai Sea, counterclockwise circulation in the northern Yellow Sea east of the Shandong Peninsula, flow southward off the Chinese coast between the 40 and 60 m depth contour, and northward flow through the Yellow Sea between the 60 and 80 m depth contour. Some differences occur near the mouth of the Yangtze and the northernmost section of the Bohai Sea. Geostrophic currents indicate excessively high flow out of the Bohai Sea during days 96 and 97. The 5 m currents indicate flow toward the southern coast of Bohai Sea in response to the transient wind stress. Such differences are expected to occur as the geostrophic balance depicts steady state, and large transients such as wind-driven transport will deviate from the balance. At 50 m (Plate 1c), outflow from Bohai Sea indicates better agreement with the geostrophic flow.

Along the Chinese coast during days 96–99, geostrophy indicates a southward flow in response to the sea level gradient along the coast. Flow turns eastward south of the Yangtze River mouth in the East China Sea and then turns northward into the central Yellow Sea. South of Inchon to the southern tip of Korea, southward geostrophic flow occurs during this period. However, the model currents at 5 m (Plate 1b) indicate a weak southward flow at the coast and a strong northward flow off the coast caused by the Ekman transport (Plate 2b).

6. Conclusions

We use a 3-D numerical model with realistic atmospheric forcing and climatological boundary forcing to simulate the circulation in the Yellow and East China Seas. We examine how the model simulates the general circulation in the region and how it responds to northerly wind bursts, which occur frequently during winter months. This model recreates elevation and pressure responses to wind events reasonably well, and the vertically integrated results compare well with previous barotropic models. Response to northerly wind events in the model is similar to such events observed in in situ measurements. Even though the numerical model is not an exact representation of the ocean circulation, it does lend insight and guidance to understanding the flow patterns and forcing mechanisms.

The transport in the deep trough of the Yellow Sea indicates a mean northward flow to counter the southward mean surface flow induced by wind stress. Strong northerly wind stress events produce elevation gradients and thus pressure forcing into the

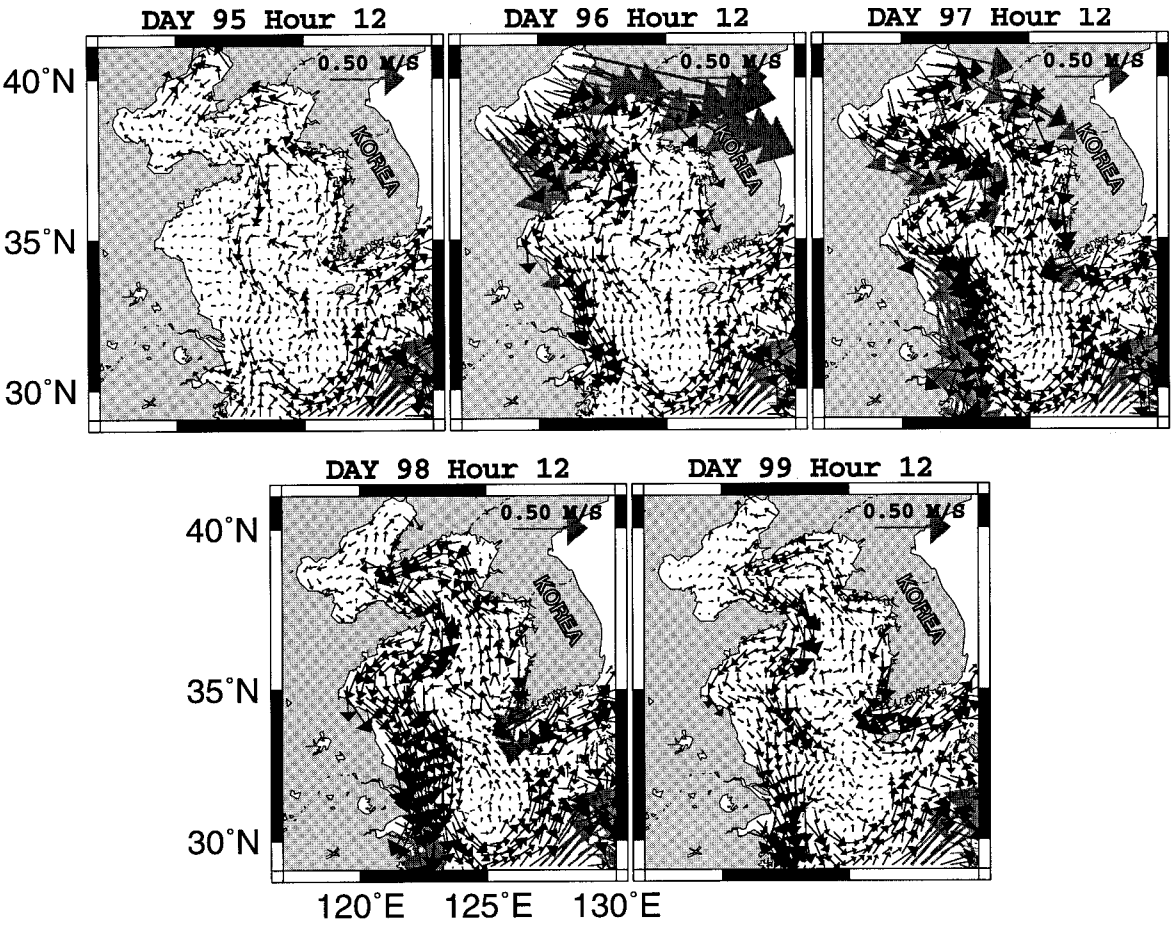

Figure 8. Geostrophic velocity computed from model elevations (Plate 1) for days 95–99 (m s^{-1}). Vectors with magnitude >0.3 m s^{-1} are shaded.

Yellow Sea. Within 24 hours of the peak northerly wind stress anomaly the peak northward current anomaly in the Yellow Sea trough occurs. The northerly wind events generate the pressure gradient by forcing water from the Bohai Sea and northern Yellow Sea. The transport out of the Bohai Sea is seen as a southward transport along the Chinese coast. In addition, Ekman transport generates a set up along the Chinese coast, and this set up intensifies the southward flow through geostrophy. Peak transport along the Chinese coast is observed 9 hours after the peak wind stress, and the maximum set down in the Bohai Sea occurs 12 hours after the peak wind stress. The transport along the Korean coast is weakly southerly and is usually not strongly related to the northerly wind events. The mean February flow at depth showed a northward flow in the Yellow Sea trough from Cheju to the Bohai Sea. This mean flow does not imply a steady northward flow but instead represents the net effect of frequent northward flow events of 1 to 2 days duration. One northward flow event is not likely to transport much heat or salt northward in the trough as the duration is rather short and frequently brief southward flow follows the northward flow. However, frequent northward flow events, some with little slack time between events, can result in a northward drift of heat and salt.

Ekman transport has a large effect near the coastal areas. The Chinese coastal current is intensified during the northerly wind events. The Korean coastal current is strongly controlled by the local offshore wind stress in addition to the geostrophic currents. In general, the forces in the depth-averaged velocity are in geostrophic balance. Significant deviations from geostrophy do occur, particularly in response to short-term transients and Ekman transport. Bottom friction and nonlinear advection of momentum play secondary roles.

The largest difference between the barotropic and baroclinic results is in the transport of the deep (50 m) waters. The northward transport at 50 m peaks soon after the peak southward pressure gradient. In previous barotropic studies the northward transport peaks after the wind stress has relaxed. Thus the surface transport is largely driven by wind stress and Ekman dynamics, while the bottom currents are not directly forced by the wind but by the pressure gradient generated by the wind.

We did not expressly examine the role played by the open boundaries in this study. However, we refer to other papers using the same numerical model used here to give some insight as to how boundary forcing effects the Yellow Sea. *Mask et al.* [1998] showed that there was a weak northward flow in the Yellow Sea trough even without wind forcing. Winds intensified the currents, acted as a steering force on the currents, and added a pulse-like flow to the currents. *Jacobs et al.* [2000] applied tracers to the inflow at the Taiwan Strait and Kuroshio south of Taiwan to examine how water entering through these open boundaries may be distributed throughout the region. The tracers were treated numerically just like the temperature and salinity, except the only source was at the western open

boundaries. Their results from tests run with and without wind forcing showed that in both cases, water from the Taiwan Strait (TWC) and the Kuroshio (KUC) found its way into the Yellow Sea. The Yangzte Relic River Valley and the Yellow Sea trough were the areas where the TWC and KUC waters were found. Without wind forcing, weak northward flow occurs in the Yellow Sea trough with southward coastal currents along the Chinese and Korean coast. This suggests that the coastal currents are a mass balance response to the northward flow in the trough. Northerly winter winds strengthen the southward coastal currents. Increased northward flow in the trough then becomes a mass balance response to the pressure fields set up by the winds.

Acknowledgments. This work was sponsored by the Office of Naval Research (program element 601153N) as part of the projects "Yellow and East China Seas Response to Winds and Currents" and "Dynamical Linkage of the Asian marginal Seas."

References

Beardsley, R. C., R. Limeburner, D. Hu, and K. Le, Structure of Changjiang River Plume in the East China Sea during June, 1980, in *Proceedings of International Symposium on Sedimentation on the Continental Shelf, with Special Reference to the East China Sea*, edited by L. Yuru and N. Ostenso, pp. 243–260, China Ocean, Beijing, 1983.

Beardsley, R. C., R. Limeburner, D. Hu, and G. A. Cannon, Discharge of the Changjiang (Yangtze River) into the East China Sea, *Cont. Shelf Res*., *4*, 57–76, 1985.

Blumberg, A., and G. Mellor, A description of a three-dimensional coastal ocean circulation model, in *Three-Dimensional Coastal Ocean Modes*, *Coastal Estuarine Sci*., vol. 4, edited by N. S. Heaps, pp. 1–16, AGU, Washington, D.C., 1987.

Chen, C., R. C. Beardsley, R. Limeburner, and K. Kim, Comparison of winter and summer hydrographic observations in the Yellow Sea and East China Seas and adjacent Kuroshio during 1986, *Cont. Shelf Res*., *14*, 909–929, 1994.

Choi, B., Note on currents driven by a steady uniform wind stress on the Yellow Sea and the East China Sea, *Mer*, *20*, 65–74, 1982.

Fang, G., B. Zhao, and Y. Zhu, Water volume transport through the Taiwan Strait and the continental shelf of the East China Sea measured with current meters, in *Oceanography of the Asian Marginal Seas*, edited by K. Takano, pp. 345–358, Elsevier Sci., New York, 1991.

Gill, A., *Atmosphere-Ocean Dynamics*, *Int. Geophys. Ser*., vol. 30, Academic, San Diego, Calif., 1982.

Hogan, T. F., and T. E. Rosmond, The description of the Navy Operational Global Atmospheric Prediction System, *Mon. Weather Rev*., *119*, 1786–1815, 1991.

Hsueh, Y., Recent current observations in the Eastern Yellow Sea, *J. Geophys. Res*., *93*, 6875–6884, 1988.

Hsueh, Y., and D. Yuan, A numerical study of currents, heat advection, and sea-level fluctuations in the Yellow Sea in winter 1986, *J. Phys. Oceanogr*., *27*, 2313–2326, 1997.

Hsueh, Y., R. Romea, and P. DeWitt, Wintertime winds and coastal sea-level fluctuations in the northeast China Sea, part 2, Numerical model, *J. Phys. Oceanogr*., *16*, 241–261, 1986.

Hu, D., Z. Ding, and Q. Xiong, A preliminary investigation of a cyclonic eddy in the northern East China Sea in summer, *Kexue Tongbao Engl. Transl*., *25*, 57–60, 1980.

Hur, H. B., G. A. Jacobs, and W. J. Teague, Monthly variations of water masses in the Yellow and East China Seas, November 6, 1998, *J. Oceanogr*., *55*, 171–184, 1999.

Jacobs, G. A., R. H. Preller, S. K. Riedlinger, and W. J. Teague, Coastal wave generation in the Bohai Bay and propagation along the Chinese coast, *Geophys. Res. Lett*., *25*, 777–780, 1998a.

Jacobs, G. A., W. J. Teague, S. K. Riedlinger, R. H. Preller, and J. P. Blaha, Sea surface height variations in the Yellow and East China Seas, 2, SSH variability in the weekly and semiweekly bands, *J. Geophys. Res*., *103*, 18,479–18,496, 1998b.

Jacobs, G. A., H. B. Hur, and S. K. Riedlinger, Yellow and East China Seas response to winds and currents, *J. Geophys. Res*., *105*, 21,947–21,968, 2000.

Le, K., M. Feng, and Y. Wang, A numerical study of the wintertime circulation in the Bohai and Huanghai Seas, *Chin. J. Oceanol. Limnol*., *11*, 149–160, 1993.

Lee, S.-H., and H.-Y. Choi, A numerical model study of residual tidal currents in the mideastern Yellow Sea: Initial stratification, *Yellow Sea*, *3*, 58–70, 1997.

Lie, H.-J., A note on water masses and general circulation in the Yellow Sea (Hwanghae), *J. Oceanol. Soc. Korea*, *19*, 187–194, 1984.

Lie, H.-J., Tidal fronts in the southern Hwanghae (Yellow Sea), *Cont. Shelf Res*., *9*, 527–546, 1989.

List, R. J., *Smithsonian Meteorological Tables*, vol. 114, 6th ed., 527 pp., Smithson. Inst., Washington, D. C., 1958.

Liu, S., S. Xingqiang, Y. Wang, and S. Han, Preliminary analysis of distribution and variation of perennial monthly mean water masses in the Bohai Sea, the Huanghai Sea, and the East China Sea, *Haiyang Xuebao Zhongwenban*, *11*, 483–498, 1992.

Mao, H., D. Hu, B. Zhao, and Z. Ding, Mesoscale eddy movement in the northern East China Sea, *Chin. J. Oceanol. Limnol*., *1*, 237–247, 1983.

Mask, A. C., J. J. O'Brien, and R. H. Preller, Wind-driven effects on the Yellow Sea Warm Current, *J. Geophys. Res*., *103*, 30,713–30,729, 1998.

Miao, J., and X. Liu, Some numerical experiments of the dynamic of the wintertime circulation in the northern Huanghai Sea and the Bohai Sea, *Haiyang Xuebao Zhongwenban*, *8*, 327–336, 1989.

Morel, A., and D. Antoine, Heating rate within the upper ocean in relation to its bio-optical state, *J. Phys. Oceanogr*., *24*, 1652–1665, 1994.

Nitani, H., Beginning of the Kuroshio, in *Kuroshio: Physical Aspects of the Japan Current*, edited by H. Stommel and K. Yoshida, pp. 138–142, Univ. of Wash. Press, Seattle, 1972.

Parkinson, C., and W. Washington, A large-scale numerical model of sea ice, *J. Geophys. Res*., *84*, 311–337, 1979.

Qingge, L., P. Delu, P. Yuqiu, L. Bannehr, and G. Warnecke, Derivation of sea surface current field from sequential satellite images of the East China Sea, *Haiyang Xuebao Zhongwenban*, *17*, 459–468, 1998.

Reed, R., On estimation insolation over the ocean, *J. Phys. Oceanogr*., *7*, 482–485, 1977.

Seung, Y. H., J. H. Chung, and Y. C. Park, Oceanographic studies related to the tidal front in the mid-Yellow Sea off Korea: Physical aspect, *Han'guk Haeyang Hakhoechi*, *25*, 84–95, 1990.

Shin, S. I., and Y. H. Seung, A numerical modeling of tidal front in the mid-Yellow Sea off Korea using a concept of mixing rate, *Han'guk Haeyang Hakhoechi*, *28*, 121–131, 1993.

Su, Y., and X. Weng, Water masses in China Sea, in *Oceanology of China Sea*, vol. 1, pp. 3–16, Kluwer Acad., Norwell, Mass., 1994.

Teague, W. J., H. T. Perkins, Z. R. Hallock, and G. A. Jacobs, Current and tide observations in the southern Yellow Sea, *J. Geophys. Res*., *103*, 27,783–27,793, 1998.

Uda, M., The results of simultaneous oceanographical investigations in the Japan Sea and its adjacent waters in May and June, 1932, *Jpn. Imperial Fish. Exped. Stn*., *5*, 57–190, 1934.

Walker, N., and R. Mey, Ocean/atmosphere heat fluxes within the Agulhas Retroflection Region, *J. Geophys. Res*., *93*, 15,473–15,483, 1988.

Wang, J., and Y. Yuan, Numerical modeling of wintertime circulation in the East China Sea, *Chin. J. Oceanol. Limnol*., *6*, 300–319, 1988.

Zhao, B., and G. Fang, Estimation of water volume transports through the main straits of the East China Sea, *Haiyang Xuebao Zhongwenban*, *10*, 1–13, 1991.

Zheng, Q., and V. Klemas, Determination of winter temperature patterns, fronts, and surface currents in the Yellow Sea and East China Sea from satellite imagery, *Remote Sens. Environ*., *12*, 201–218, 1982.

G. A. Jacobs and S. K. Riedlinger, Naval Research Center, Code 7322, Stennis Space Center, MS 39529. (horton@nrlssc.navy.mil)

(Received February 16, 1999; revised December 30, 1999; accepted May 22, 2000.)